Nanoscale Research Letters

NANO EXPRESS Open Access

Stable High-Efficiency Two-Dimensional Perovskite Solar Cells Via Bromine Incorporation

Feng Han[1*], Wenyao Yang[2], Hao Li[3] and Lei Zhu[4]

Abstract

Two-dimensional (2D) organic-inorganic perovskites as one of the most important photovoltaic material used in solar cells have attracted remarkable attention. These 2D perovskites exhibit superior environmental stability and wide tunability of their optoelectronic properties. However, their photovoltaic performance is far behind those of traditional three-dimensional (3D) perovskites. In this work, we demonstrate the power conversion efficiency (*PCE*) of 2D perovskite solar cells (PVSCs) is greatly improved from 3.01% for initial to 12.19% by the incorporation of $PbBr_2$. The enhanced efficiency is attributed to superior surface quality, enhanced crystallinity, and the resulting reduced trap-state density. Furthermore, $PbBr_2$ incorporated devices without encapsulation show excellent humidity stability, illumination stability, and thermal stability. This work provides a universal and viable avenue toward efficient and stable 2D PVSCs.

Keywords: Two-dimensional perovskite, Bromine incorporation, Stability

Introduction

During the past decade, the hybrid organic-inorganic perovskites have drawn significant attention as promising photo-voltage materials due to their easy preparation process and excellent optoelectronic characteristics, such as small exciton binding energy, appropriate bandgap, great light absorption, and long exciton diffusion length [1–6]. At present, the highest certified *PCE* has exceeded 25% of 3D PVSCs [7]. Unfortunately, the stability issue of 3D perovskite hinders the commercial application of perovskite solar cells. For example, $CH_3NH_3PbI_3$ ($MAPbI_3$) perovskite will degrade rapidly when exposed to light for long periods of time or exposed to moisture [8, 9]. This problem prompted researchers to work hard to improve the stability of perovskite materials.

Recently, 2D perovskite $(RNH_3)_2A_{n-1}M_nX_{3n+1}$ (Ruddlesden-Popper phase) have been developed due to their outstanding moisture resistance, wherein R is a long-chain organic group or bulky organic group, A stands for small organic cation (MA^+, FA^+, or Cs^+), M corresponds to the B-cation in the three-dimensional perovskite (i.e., Pb^{2+} and Sn^{2+}), X is halide anion (I^-, Br^- and Cl^-), and n is the number of octahedrons in each individual perovskite layer which defined the number of 2D perovskite [10–17]. Owing to the stronger van der Waals interaction between the blocked organic molecules and the $[MX_6]^{4-}$ unit, 2D perovskite exhibits better stability than 3D perovskite [10]. However, the large exciton binding energy of 2D perovskite makes exciton dissociation more difficult [18]. Meanwhile, the insulation of the organic spacer layer hinders the transport of carriers, resulting in a reduction in photogenerated current [12]. Therefore, the PCE of 2D PVSCs lags far behind that of their 3D counterparts.

Different methods have been implemented to improve the performance of 2D PVSCs, including additive engineering [19–24], component regulation [25–33], interfacial engineering [34–37], and preparation process [38–40]. Halogen ions show great potential to improve the performance of the device in 3D PVSCs. For example, a small amount of chloride in 3D perovskite can extend the crystal crystallization time, change the crystal growth direction,

* Correspondence: hfzy083078@163.com
[1]Xi'an Technological University, Xi'an 710021, People's Republic of China
Full list of author information is available at the end of the article

reduce the density of trap states, and increase the diffusion length of photo-generated carriers [41–44]. Meanwhile, previous work proves that a small amount of bromine doped 3D perovskite enhances the stability, suppresses ion migration, and reduces trap-state density [45]. Considering the composition of 2D perovskite, it is necessary to carry out research on halogen regulation. However, only limited work has been carried on the influence of 2D perovskite halogen regulation on device performance. Liu and his coworker have found that chloride plays a critical role to improve perovskite morphology. By regulating the chloride ratio of the precursor solution, the 2D perovskite film with increased grain size, enhanced crystallinity, and uniform surface was obtained. As results, the PCE of 2D PVSCs with excellent stability was remarkably improved from 6.52 to 12.78% [46]. These results confirm that halogen regulation can improve the performance of 2D PVSCs.

In this work, we investigated the influence of bromine on the opto-electronic properties of the 2D perovskite by using n-butylamine (BA) spacer. Bromine was incorporated by using lead (II) bromide ($PbBr_2$). It is demonstrated that the incorporation of an appropriate amount of bromine is able to facilitate the formation of high-quality 2D perovskite film, which results in the reduced defect states of 2D perovskite film and enhanced photovoltaic performance of 2D PVSCs. The PCE of 2D PVSCs is boosted from 3.66 to 12.4%. More interestingly, the optimal 2D PSVCs devices exhibit a significant improvement in humidity, illumination, and thermal stabilities.

Method

Materials and Solution Preparation

Lead (II) iodide (PbI_2), $PbBr_2$, n-butylammonium iodide (BAI), methylamine iodide (CH_3NH_3I, MAI), PEDOT:PSS (4083) aqueous solution, phenyl-C61-butyric acid methyl ester ($PC_{61}BM$), and bathocuproine (BCP) were purchased from Xi'an Polymer Light Technology Cory. N,N-dimethylformamide (DMF), dimethyl sulfoxide (DMSO), and chlorobenzene were ordered from Sigma-Aldrich. Isopropanol was purchased from You Xuan Trade Co., Ltd. All reagents and solvents were used as received. The 2D perovskite $BA_2MA_4Pb_5I_{16-10x}Br_{10x}$ (n = 5, x = 0, 5, 10, or 15%) precursor solution (0.8 M) was fabricated by adding BAI, MAI, PbI_2, and $PbBr_2$ with a molar ratio of 0.4:0.8:1-x:x in the mixed solvent of DMSO and DMF in 1:15 volume ratio.

Device Fabrication

The indium tin oxide (ITO) substrates were cleaned by sequential sonication in detergent, acetone, absolute ethyl alcohol, and deionized water for 15 min each. The ITO substrates were dried in N_2 flow and cleaned by UV–O_3 treatment for 15 min. PEDOT:PSS aqueous solution was then spin-coated onto the ITO substrates under 5000 rpm for 30 s, followed by annealing at 150 °C for 15 min in air. Subsequently, the PEDOT:PSS/ITO substrates were transferred into a nitrogen glove box. The 2D perovskite solutions with different bromine content were spin-coated onto the preheated PEDOT:PSS/ITO substrates by a spin-coating process at 5000 rpm for 20 s and then annealing at 100 °C for 10 min. After annealing, the prepared PCBM solution (20 mg/mL in chlorobenzene) and BCP solution (0.5 mg/mL in isopropanol) were posited above on 2D perovskite film at 2000 rpm for 30 s and 5000 rpm for 30 s, respectively. Finally, thermally evaporation was implemented to prepare the electrodes Ag with thickness of 70 nm.

Measurement and Characterization

The scanning electron microscope (FEI-Inspect F50, Holland), atomic force microscopy (Cypher S), and X-ray diffraction (Bruker D8 ADVANCE A25X) measurements were conducted based on the structure of ITO-etched glass/PEDOT:PSS/2D perovskite. The UV-visible absorption spectrum of 2D perovskite films on glasses was measured by Shimadzu 1500 spectrophotometer. PL spectrum was collected by Fluo Time 300 (Pico Quant) spectrofluorometer. The current density-voltage (J-V) characteristics of 2D PVSCs were collected using a Keithley 2400 Sourcemeter under AM 1.5G sun intensity irradiated by a Newport Corp solar simulator. The active area of the device is 0.04 cm^2. The J-V curves were measured in the reverse (from 1.2 to 0 V) and forward (from 0 to 1.2 V) directions with a scanning rate of 0.23 V/s, fixed voltage interval of 0.0174 mV, and dwelling time of 10 ms. Dark current-voltage curves were measured in the same way under the dark condition.

Results and Discussion

The 2D perovskite films incorporated different amounts of bromine were prepared by a previously reported hot-casting method. By using this method, substrates are preheated to favor crystallization and orientation [40]. To investigate the effects of different amounts of $PbBr_2$ in the 2D perovskite precursor solutions on the morphology of resultant film, a scanning electron microscope (SEM) and atomic force microscopy (AFM) measurements were carried out. As shown in Fig. 1a, the 2D perovskite $BA_2MA_4Pb_5I_{16-10x}Br_{10x}$ film without bromine incorporation (x = 0%, denoted as control perovskite) exhibits a poor morphology with big cracks, indicating the low coverage and inferior compactness. The cracks are disappeared in the 2D perovskite film with 5 mol% $PbBr_2$ content (x = 5%, denoted as perovskite-5%). However, the perovskite-5% film still shows some pinholes (Fig. 1b). In the case of the 2D perovskite film with 10 mol% $PbBr_2$ content (x = 10%, denoted as perovskite-10%), the film surface becomes uniform and compact without any cracks or pinholes (Fig. 1c). As the $PbBr_2$ content is further increased to 15 mol% (x = 15%, denoted as perovskite-15%),

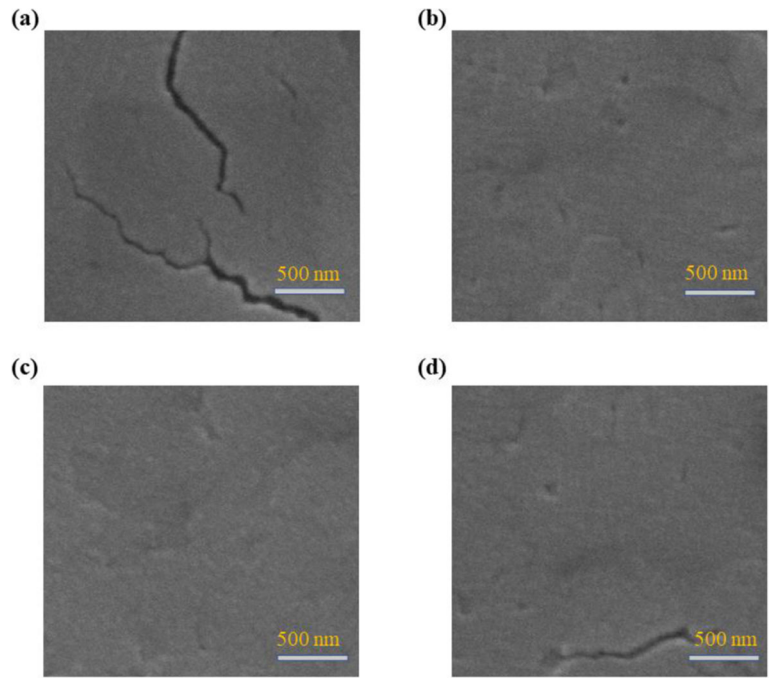

Fig. 1 SEM images of $BA_2MA_4Pb_5I_{16-10x}Br_{10x}$ films based on **a** 0% $PbBr_2$, **b** 5% $PbBr_2$, **c** 10% $PbBr_2$, and **d** 15% $PbBr_2$

cracks appeared in the film again (Fig. 1d). The AFM images of 2D perovskite film with various amounts of $PbBr_2$ are shown in Fig. 2a–d, which are consistent with the SEM results. The control perovskite film shows a rough surface with a high root-mean-squared roughness (RMS) value of 51.2 nm. The partial replacement of iodine with bromine greatly reduces the RMS value to 21.3 nm for perovskite-5% and 23.1 nm for perovskite-15%, respectively. Especially, the perovskite-10% film exhibits a quite smooth surface with the lowest RMS value of 10.7 nm due to the disappearance of cracks and pinholes. The above results indicate that incorporating an appropriate amount of bromine is beneficial to improve the uniformity and surface coverage of the 2D perovskite film. It is well known that cracks and pinholes in the film can lead to strong energetic disorder, cause recombination, impede charge transport, and weaken photovoltaic performance [47]. Therefore, obtaining a uniform and well-covered perovskite film is essential to improve device efficiency.

To investigate the impact of bromine on the crystal phase and crystallinity of 2D perovskite films, X-ray diffraction (XRD) measurements were performed. As shown in Fig. 2e, all films show two distinctive diffraction peaks at around 14.5° and 28.4°, which can be assigned to (111) and (202) crystallographic planes, respectively. Previous studies have suggested that both the (111) and (202) orientation allow the $[(MA)_{n-1}Pb_nI_{3n+1}]^{2-}$ slabs grow in vertical alignment to the PEDOT:PSS/ITO substrate [13, 23, 24]. Therefore, limited replacement of iodine with bromine is conducive to the formation of vertically oriented 2D perovskite film, as evidenced by the preferred intensity increase in the (111) and (202) peaks [48]. The vertical oriented 2D perovskite film allows more efficient transport of photon-induced carriers, improving photovoltaic performance of PVSC [23, 24]. On the one hand, the diffraction peaks at around 14.5° and 28.4° both become stronger upon the incorporation of bromine, suggesting the enhanced crystallinity of the perovskite film. On the other hand, the two peaks are gradually shifted towards higher angles upon the bromine incorporation, which is due to the smaller size of the bromine ion with respect to the iodine ion that shrinks the crystal lattice [13]. These gradual shifts in diffraction peak position prove that mixed $BA_2MA_4Pb_5I_{16-10x}Br_{10x}$ perovskites are formed with bromine ion inserted in the crystal lattice. It is worth noting that all of the films show the peaks of (0 *k*0) reflections at low angles (< 10°), indicating the formation of 2D RP perovskite structures (Fig. 2f). However, the control film exhibits some diffraction peaks that could not be assigned to any typical 2D perovskite characteristic peak. The intensity of these undesired peaks is weakened upon the incorporation of bromine, giving rise to the lowest intensity in perovskite-10% film. This phenomenon suggests that the incorporation of moderate bromine can inhibit the formation of the impurity phases in the 2D perovskite film.

Furthermore, the absorbance and photoluminescence (PL) measurements were carried out to understand the influence of bromine incorporation on the film optical

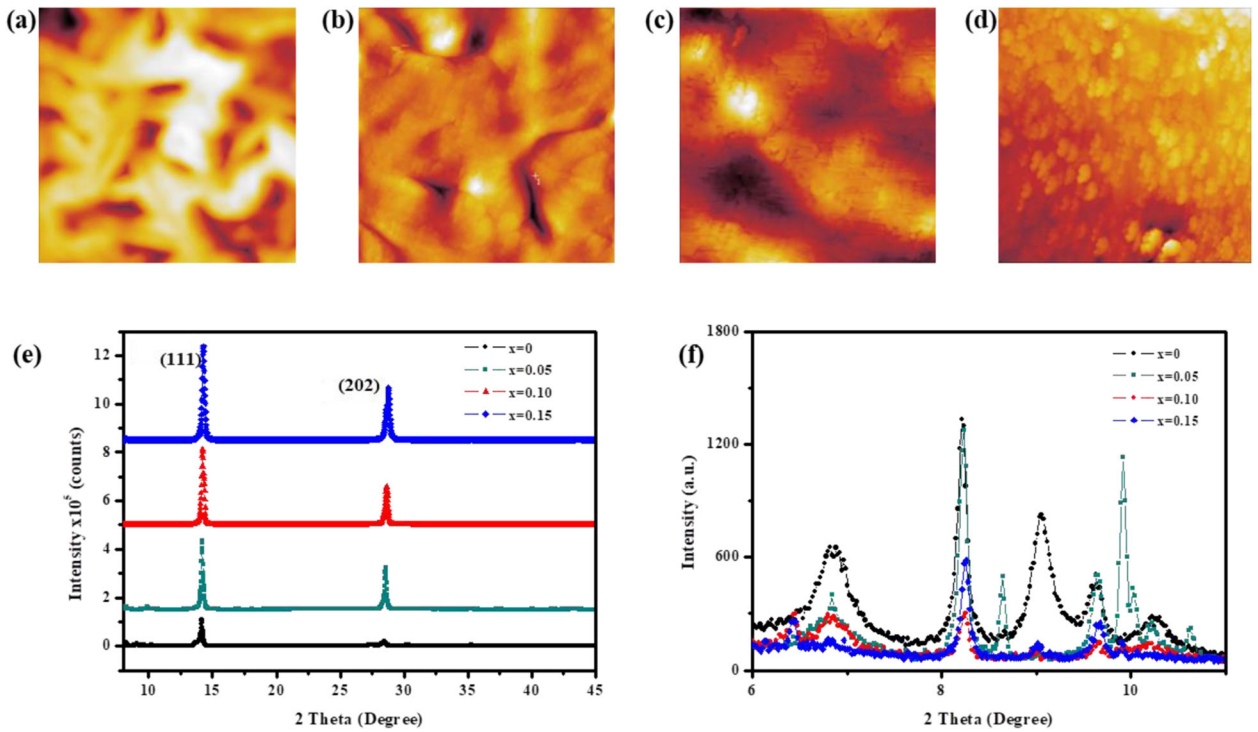

Fig. 2 AFM images of $BA_2MA_4Pb_5I_{16-10x}Br_{10x}$ films based on **a** 0% $PbBr_2$, **b** 5% $PbBr_2$, **c** 10% $PbBr_2$, and **d** 15% $PbBr_2$. X-ray diffraction patterns (**e**) and corresponding local enlarged image (**f**) of $BA_2MA_4Pb_5I_{16-10x}Br_{10x}$ films with various amounts of $PbBr_2$

properties, as summarized in Fig. 3a–c. Figure 3a shows the UV-visible absorption spectra of the 2D perovskite film with various amounts of $PbBr_2$. All these films show distinctive exciton absorption peaks in the absorption spectra, which are assigned to 2D phases with n = 2, 3, and 4, although nominally prepared as "n = 5." The perovskite-10% exhibits the enhanced absorbance intensity, resulting from a dense and uniform nature of the resultant film, as evidenced by the SEM and AFM images. Besides, the absorption edge of $BA_2MA_4Pb_5I_{16-10x}Br_{10x}$ has a blue shift with the increase of x value, which proves the widening of bandgap [49]. Figure 3b presents the steady-state PL spectra of the 2D perovskite films deposited on glass substrates. As compared to the control sample showing the weakest PL signal, either perovskite-15% sample or perovskite-5% sample exhibits the increased PL signal, while the perovskite-10% sample shows the strongest PL signal. Remarkable PL enhancement is observed after incorporating bromine, indicating the reduced trap-state density in the $PbBr_2$ treated films. Figure 3c displays the time-resolved PL decay spectra of the $BA_2MA_4Pb_5I_{16-10x}Br_{10x}$ films spin-coated on glass substrates, which also proves the reduction of trap-state density in perovskite with the incorporation of bromine. The time-resolved PL curves were fitted with a two-exponential equation (Eq. (1)) containing a fast decay and a slow decay process, and the fitting parameters are summarized in Table 1. The fast decay (τ_1) is considered to be the result of the quenching of carriers transport in the perovskite domain, and the slow decay (τ_2) is the result of radiative recombination [50]. The average lifetime (τ) of 2D perovskite films are calculated according to Eq. (2). The perovskite-10% film presents the longest τ of 3.47 ns as compared to other films (i.e., 0.9 ns, 2.72 ns, and 1.31 ns for control film, perovskite-5% film, and perovskite-15% film, respectively), suggesting a slower recombination process with less defects.

$$I(t) = \mathrm{A}_1 \exp\left(-\frac{t}{\tau_1}\right) + \mathrm{A}_2 \exp\left(-\frac{t}{\tau_2}\right) \quad (1)$$

$$\tau = A_1 \times \tau_1 + A_2 \times \tau_2 \quad (2)$$

In addition, to investigate whether reduced defect states arise from the $PbBr_2$ when the 2D perovskite films are assembled in a PVSC structure, dark current-voltage curves of the corresponding devices were also collected (Fig. 3d). The dark current of the device based on the perovskite-10% film is much lower than that of the device based on the control film at the same voltage. The lower dark current of the device based on the perovskite-10% film indicates that the reduced defect states are indeed contributed by the bromine incorporation.

It is shown $PbBr_2$ in 2D perovskite films induced improved morphology, crystallinity, and opto-electronic

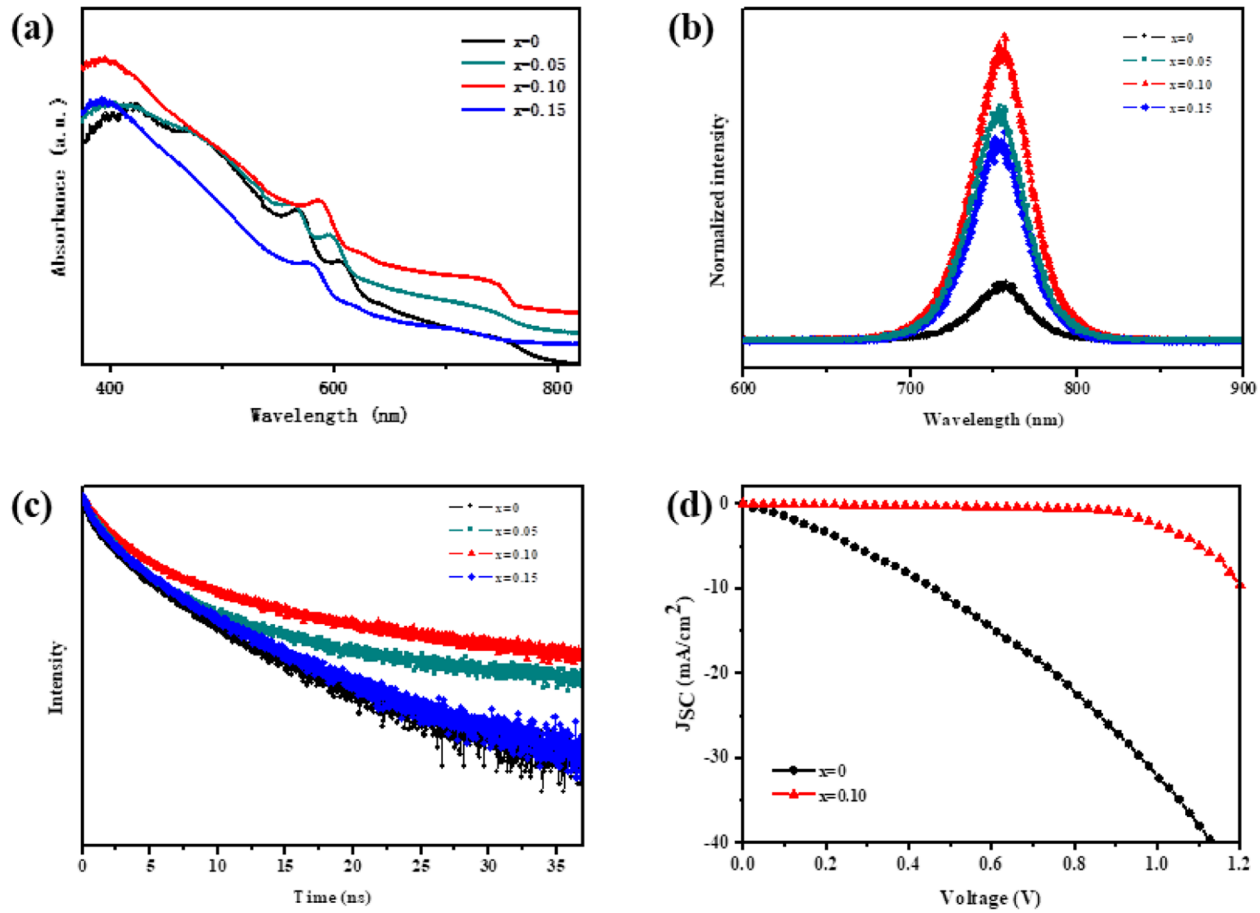

Fig. 3 **a** Absorption spectra, **b** steady-state PL spectra, and **c** time-resolved PL curves of $BA_2MA_4Pb_5I_{16-10x}Br_{10x}$ film with various amounts of $PbBr_2$ spin-coated on glass substrates. **d** Dark current-voltage measurements of PVSCs based on the $BA_2MA_4Pb_5I_{16-10x}Br_{10x}$ film with various amounts of $PbBr_2$

properties. We fabricated PVSC devices with the planar p-i-n architecture as indium tin oxide (ITO)/PEDOT:PSS/$BA_2MA_4Pb_5I_{16-10x}Br_{10x}$/PCBM/BCP/Ag. The *J-V* curves and the related parameters of the best-performing devices are shown in Fig. 4a and Table 2. The PVSCs based on the control perovskite film yielded a poor device performance, showing a champion *PCE* of 3.01% with an open-circuit voltage (V_{oc}) of 0.89 V, a short-circuit current density (J_{sc}) of 8.28 mA/cm^2, and a fill factor (*FF*) of 40.79%. The introduction of bromine into the perovskite precursor remarkably increases the *PCE* of the device (Fig. 4a). The highest *PCE* of 12.19% with a V_{oc} of 1.02 V, a J_{sc} of 17.86 mA/cm^2, and a fill factor (*FF*) of 66.91% was obtained in the 10 mol% $PbBr_2$-treated device compared to 8.88% in the 5 mol% $PbBr_2$-contained device and 7.85% in the 15 mol% $PbBr_2$-contained device. In order to more accurately compare the performance of these devices, 20 devices for each case were fabricated. From statistical data (Fig. S1, Supporting Information), the device with 10 mol% bromine shows the relatively higher V_{oc} and *FF*, which is ascribed to the reduced trap-state density resulting from high-quality perovskite film, as discussed in Fig. 3b–d. The higher V_{oc} in Br-contained devices can also attribute to the increased bandgap. The bandgap of the $BA_2MA_4Pb_5I_{16-10x}Br_{10x}$ increases with the increasing $PbBr_2$ ratio, as evidenced by Fig. 3a [49]. Thus, the 15 mol% $PbBr_2$-contained device shows the highest V_{oc}. Moreover, the high J_{sc} in 10 mol% $PbBr_2$-contained device can attribute to the increased light absorption and the efficient charge transport, as discussed above. The hysteresis of the devices based on the control perovskite film and perovskite-10% film was investigated by scanning the *J-V* curves in different directions (Fig. 4c and Fig. S2). The device based on

Table 1 Time-resolved PL parameters of $BA_2MA_4Pb_5I_{16-10x}Br_{10x}$ films spin-coated on glass substrates

Sample	A_1	τ_1 (ns)	A_2	τ_2 (ns)	τ (ns)
0 (x = 0)	0.86	0.49	0.14	3.45	0.90
5 (x = 0.05)	0.80	1.32	0.20	6.08	2.72
10 (x = 0.10)	0.75	1.59	0.25	9.12	3.47
15 (x = 0.15)	0.83	0.76	0.17	4.04	1.31

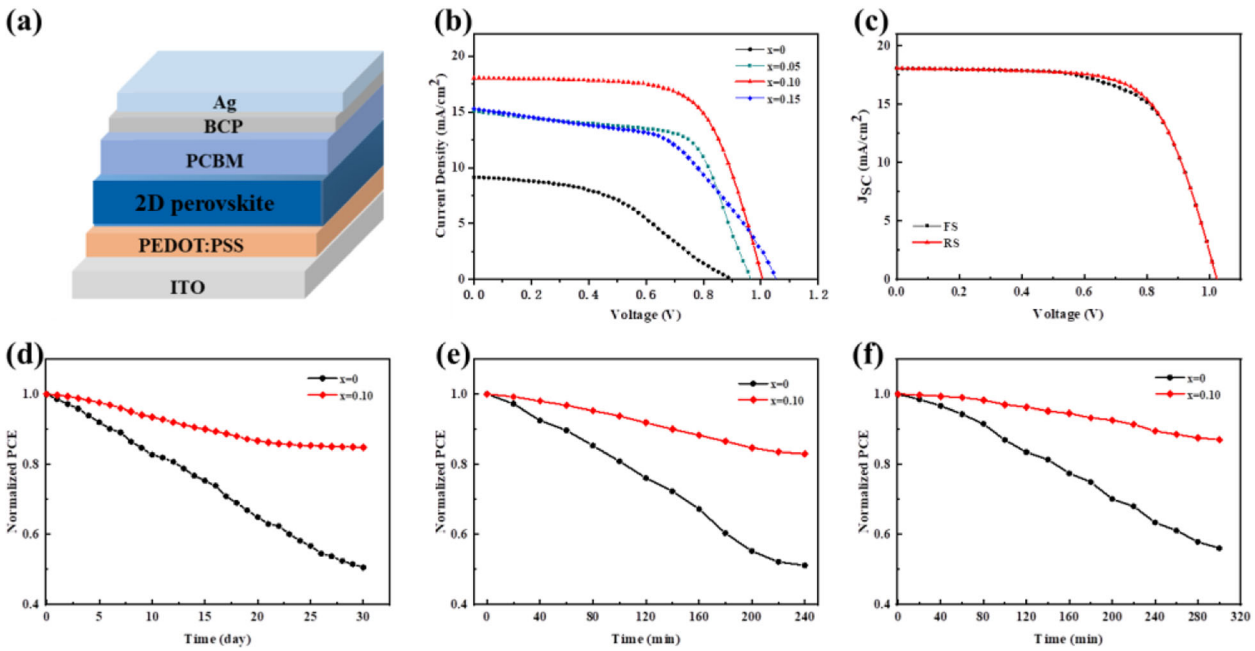

Fig. 4 **a** The device architecture of PVSC. **b** *J-V* curves of PVSCs based on $BA_2MA_4Pb_5I_{16-10x}Br_{10x}$ films with various amounts of $PbBr_2$. **c** *J-V* curves of the best-performing device at different scan directions. **d** Humidity stability, **e** illumination stability, and **f** thermal stability of the unsealed device without and with 10 mol% $PbBr_2$

the perovskite-10% exhibits slight hysteresis while serious hysteresis characteristic was observed in the device based on the control perovskite, indicating again the significant reduced defect states in the former case.

Furthermore, the incorporation of $PbBr_2$ can effectively enhance the humidity, illumination, and thermal stability of the 2D PVSCs. The unsealed control device and device based on perovskite-10% were exposed to a relative humidity level of 45–60% at 25 °C for the humidity stability testing. The *PCE* of the control device declines to 50% of its original value within 30 days while the device based on perovskite-10% still maintains 85% of its initial efficiencies under identical conditions (Fig. 4d). Interestingly, the introduction of $PbBr_2$ also enhances the illumination stability of the PVSCs. After being irradiated continuously under AM 1.5G sun intensity for 240 min, the devices retain more than 80% of the original *PCE* for perovskite-10% while only less than 50% for the control perovskite (Fig. 4e). The enhancement of thermal stability also confirmed by measurement. Both the control device and perovskite-10% device were thermally annealed at 85 °C in nitrogen atmosphere without encapsulation. As shown in Fig. 4f, the perovskite-10% device retains 83% of its initial *PCE* after 300 min, which is much higher than that of the control device (54%).

Table 2 Photovoltaic parameters of the champion devices based on $BA_2MA_4Pb_5I_{16-10x}Br_{10x}$ films with various amounts of bromine

Sample	V_{OC} (V)	J_{SC} (mA/cm^2)	*FF* (%)	*PCE* (%)
$x = 0$	0.89	8.28	40.79	3.01
$x = 0.05$	0.95	14.84	63.02	8.88
$x = 0.10$	1.02	17.86	66.91	12.19
$x = 0.15$	1.06	14.59	50.73	7.85

Conclusion

In conclusion, we demonstrated that incorporating suitable bromine in precursor solution can improve the morphology of 2D perovskite films with enhanced crystallinity, leading to an improvement in opto-electronic properties in terms of absorbance and trap density. The outstanding film quality and opto-electronic properties yield an obvious enhancement in *PCE* from 3.01 to 12.19%. Moreover, the bromine incorporation enhances the tolerance of PVSCs to humidity, illumination, and thermal stability. These results prove that incorporating bromine is crucial to achieving stable high-performance 2D PVSCs.

Additional File

Additional file 1: Fig. S1. Statistic distribution for (a) V_{oc}, (b) J_{sc}, (c) *FF*, and (d) *PCE* of 2D PVSCs based on $BA_2MA_4Pb_5I_{16-10x}Br_{10x}$ films with

various amounts of $PbBr_2$. **Fig. S2.** J–V curves of the control device at different scan directions.

Abbreviations

3D: Three-dimensional; 2D: Two-dimensional; *PCE*: Power conversion efficiency; PVSCs: Perovskite solar cells; $PbBr_2$: Lead (II) bromide; PbI_2: Lead (II) iodide; BAI: N-butylammonium iodide; MAI: Methyl-ammonium iodide; $PC_{61}BM$: Phenyl-C61-butyric acid methyl ester; DMSO: Dimethyl sulfoxide; BCP: Bathocuproine; ITO: Indium tin oxide; *J-V*: Current density-voltage; SEM: Scanning electron microscope; AFM: Atomic force microscopy; RMS: Root-mean-squared roughness; PL: Photoluminescence; V_{oc}: Circuit voltage; J_{sc}: Short-circuit current density; *FF*: Fill factor

Acknowledgements

The authors greatly acknowledge the Xi'an Technological University, Chongqing Engineering Research Center of New Energy Storage Devices and Applications, University of Electronic Science and Technology of China, Xi'an Institute of Applied Optics, and Ceshigou Analytical Testing Company for the measurement assistance.

Authors' Contributions

F. Han and H. Li did the experiment and characterization together. W. Yang wrote the article. L. Zhu revised the article. The authors read and approved the final manuscript.

Funding

This work was partially supported by the Natural Science Foundation of Chongqing (cstc2019jcyj-msxmX0824).

Availability of Data and Materials

All the data are fully available without restrictions.

Competing Interests

The authors declare that they have no competing interests.

Author details

[1]Xi'an Technological University, Xi'an 710021, People's Republic of China. [2]Chongqing Engineering Research Center of New Energy Storage Devices and Applications, Chongqing University of Arts and Sciences, Chongqing 402160, People's Republic of China. [3]State Key Laboratory of Electronic Thin Films and Integrated Devices, and School of Optoelectronic Science and Engineering, University of Electronic Science and Technology of China (UESTC), Chengdu 610054, Sichuan, People's Republic of China. [4]Xi'an Institute of Applied Optics, Xi'an 710100, People's Republic of China.

Received: 3 August 2020 Accepted: 2 September 2020
Published online: 01 October 2020

References

1. Noh JH, Im SH, Heo JH, Mandal TN, Seok SI (2013) Chemical management for colorful, efficient, and stable inorganic-organic hybrid nanostructured solar cells. Nano Lett 13:1764–1769
2. Zhao DW, Yu Y, Wang CL, Liao WQ, Shrestha N, Grice CR, Cimaroli AJ, Guan L, Ellingson RJ, Zhu K, Zhao XZ, Xiong RG, Yan YF (2017) Low-bandgap mixed tin-lead iodide perovskite absorbers with long carrier lifetimes for all-perovskite tandem solar cells. Nat Energy 2
3. Zhang YX, Liu YC, Li YJ, Yang Z, Liu SZ (2016) Perovskite CH3NH3Pb(BrxI1-x)(3) single crystals with controlled composition for fine-tuned bandgap towards optimized optoelectronic applications. J Mater Chem C 4:9172–9178
4. Loper P, Stuckelberger M, Niesen B, Werner J, Filipic M, Moon SJ, Yum JH, Topic M, De Wolf S, Ballif C (2015) Complex refractive index spectra of CH3NH3PbI3 perovskite thin films determined by spectroscopic ellipsometry and spectrophotometry. J Phys Chem Lett 6:66–71
5. Baena JPC, Steier L, Tress W, Saliba M, Neutzner S, Matsui T, Giordano F, Jacobsson TJ, Kandada ARS, Zakeeruddin SM, Petrozza A, Abate A, Nazeeruddin MK, Gratzel M, Hagfeldt A (2015) Highly efficient planar perovskite solar cells through band alignment engineering. Energy Environ Sci 8:2928–2934
6. Stranks SD, Eperon GE, Grancini G, Menelaou C, Alcocer MJ, Leijtens T, Herz LM, Petrozza A, Snaith HJ (2013) Electron-hole diffusion lengths exceeding 1 micrometer in an organometal trihalide perovskite absorber. Science 342:341–344
7. NREL: National Center For Photovoltaics Home Page. [Online]. https://www.nrel.gov/pv/assets/pdfs/best-research-cell-efficiencies-190416.pdf. Accessed 16 February 2020.
8. Frost JM, Butler KT, Brivio F, Hendon CH, van Schilfgaarde M, Walsh A (2014) Atomistic origins of high-performance in hybrid halide perovskite solar cells. Nano Lett 14:2584–2590
9. Bryant D, Aristidou N, Pont S, Sanchez-Molina I, Chotchunangatchaval T, Wheeler S, Durrant JR, Haque SA (2016) Light and oxygen induced degradation limits the operational stability of methylammonium lead triiodide perovskite solar cells. Energy Environ Sci 9:1655–1660
10. Quan LN, Yuan M, Comin R, Voznyy O, Beauregard EM, Hoogland S, Buin A, Kirmani AR, Zhao K, Amassian A, Kim DH, Sargent EH (2016) Ligand-stabilized reduced-dimensionality perovskites. J Am Chem Soc 138:2649–2655
11. Liao Y, Liu H, Zhou W, Yang D, Shang Y, Shi Z, Li B, Jiang X, Zhang L, Quan LN, Quintero-Bermudez R, Sutherland BR, Mi Q, Sargent EH, Ning Z (2017) Highly oriented low-dimensional tin halide perovskites with enhanced stability and photovoltaic performance. J Am Chem Soc 139:6693–6699
12. Zhang X, Ren X, Liu B, Munir R, Zhu X, Yang D, Li J, Liu Y, Smilgies D-M, Li R, Yang Z, Niu T, Wang X, Amassian A, Zhao K, Liu S (2017) Stable high efficiency two-dimensional perovskite solar cells via cesium doping. Energy Environ Sci 10:2095–2102
13. Zhou N, Shen Y, Li L, Tan S, Liu N, Zheng G, Chen Q, Zhou H (2018) Exploration of crystallization kinetics in quasi two-dimensional perovskite and high performance solar cells. J Am Chem Soc 140:459–465
14. Stoumpos CC, Soe CMM, Tsai H, Nie WY, Blancon JC, Cao DYH, Liu FZ, Traore B, Katan C, Even J, Mohite AD, Kanatzidis MG (2017) High members of the 2D Ruddlesden-Popper halide perovskites: synthesis, optical properties, and solar cells of (CH3(CH2)(3)NH3)(2)(CH3NH3)(4)Pb(5)I16. Chem-Us 2:427–440
15. Mao L, Tsai H, Nie W, Ma L, Im J, Stoumpos CC, Malliakas CD, Hao F, Wasielewski MR, Mohite AD, Kanatzidis MG (2016) Role of organic counterion in lead- and tin-based two-dimensional semiconducting iodide perovskites and application in planar solar cells. Chem Mater 28:7781–7792
16. Cao DH, Stoumpos CC, Farha OK, Hupp JT, Kanatzidis MG (2015) 2D Homologous perovskites as light-absorbing materials for solar cell applications. J Am Chem Soc 137:7843–7850
17. Cohen B-E, Wierzbowska M, Etgar L (2017) High efficiency and high open circuit voltage in quasi 2D perovskite based solar cells. Adv Funct Mater 27:1604733
18. Sum TC, Mathews N (2014) Advancements in perovskite solar cells: photophysics behind the photovoltaics. Energy Environ Sci 7:2518–2534
19. Zhang X, Wu G, Yang S, Fu W, Zhang Z, Chen C, Liu W, Yan J, Yang W, Chen H (2017) Vertically oriented 2D layered perovskite solar cells with enhanced efficiency and good stability. Small 13
20. Yu S, Yan Y, Chen Y, Chábera P, Zheng K, Liang Z (2019) Correction: enabling room-temperature processed highly efficient and stable 2D Ruddlesden–Popper perovskite solar cells with eliminated hysteresis by synergistic exploitation of additives and solvents. J Mater Chem A 7:11538
21. Qing J, Liu XK, Li MJ, Liu F, Yuan ZC, Tiukalova E, Yan ZB, Duchamp M, Chen S, Wang YM, Bai S, Liu JM, Snaith HJ, Lee CS, Sum TC, Gao F (2018) Aligned and graded type-II Ruddlesden-Popper perovskite films for efficient solar cells. Adv Energy Mater 8
22. Fu WF, Wang J, Zuo LJ, Gao K, Liu F, Ginger DS, Jen AKY (2018) Two-dimensional perovskite solar cells with 14.1% power conversion efficiency and 0.68% external radiative efficiency. Acs Energy Lett 3:2086–2093
23. Zheng HL, Liu DT, Wang YF, Yang YG, Li H, Zhang T, Chen H, Ji L, Chen Z, Li SB (2020) Synergistic effect of additives on 2D perovskite film towards efficient and stable solar cell. Chem Eng J 389
24. Liu Z, Zheng H, Liu D, Liang Z, Yang W, Chen H, Ji L, Yuan S, Gu Y, Li S (2020) Controllable two-dimensional perovskite crystallization via water additive for high-performance solar cells. Nanoscale Res Lett 15:108
25. Chen YN, Sun Y, Peng JJ, Zhang W, Su XJ, Zheng KB, Pullerits T, Liang ZQ (2017) Tailoring organic cation of 2D air-stable organometal halide perovskites for highly efficient planar solar cells. Adv Energy Mater 7
26. Proppe AH, Quintero-Bermudez R, Tan H, Voznyy O, Kelley SO, Sargent EH (2018) Synthetic control over quantum well width distribution and carrier

migration in low-dimensional perovskite photovoltaics. J Am Chem Soc 140: 2890–2896
27. Tan SQ, Zhou N, Chen YH, Li L, Liu GL, Liu PF, Zhu C, Lu JZ, Sun WT, Chen Q, Zhou HP (2019) Effect of high dipole moment cation on layered 2D organic-inorganic halide perovskite solar cells. Adv Energy Mater 9
28. Lian X, Chen J, Qin M, Zhang Y, Tian S, Lu X, Wu G, Chen H (2019) The second spacer cation assisted growth of a 2D perovskite film with oriented large grain for highly efficient and stable solar cells. Angew Chem 58:9409–9413
29. Chen S, Shen N, Zhang LZ, Kong WG, Zhang LH, Cheng C, Xu BM (2019) Binary organic spacer-based quasi-two-dimensional perovskites with preferable vertical orientation and efficient charge transport for high-performance planar solar cells. J Mater Chem A 7:9542–9549
30. Zhou N, Huang BL, Sun MZ, Zhang Y, Li L, Lun YZ, Wang XY, Hong JY, Chen Q, Zhou HP (2020) The spacer cations interplay for efficient and stable layered 2D perovskite solar cells. Adv Energy Mater 10
31. Jiang YY, He XY, Liu TF, Zhao N, Qin MC, Liu JX, Jiang FY, Qin F, Sun LL, Lu XH, Jin SY, Xiao ZW, Kamiya T, Zhou YH (2019) Intralayer A-site compositional engineering of Ruddlesden-Popper perovskites for thermostable and efficient solar cells. Acs Energy Lett 4:1216–1224
32. Ren H, Yu SD, Chao LF, Xia YD, Sun YH, Zuo SW, Li F, Niu TT, Yang YG, Ju HX, Li BX, Du HY, Gao XY, Zhang J, Wang JP, Zhang LJ, Chen YH, Huang W (2020) Efficient and stable Ruddlesden-Popper perovskite solar cell with tailored interlayer molecular interaction. Nat Photonics 14:154
33. Ma C, Shen D, Ng TW, Lo MF, Lee CS (2018) 2D perovskites with short interlayer distance for high-performance solar cell application. Adv Mater 30: e1800710
34. Chen J, Lian X, Zhang Y, Yang W, Li J, Qin M, Lu X, Wu G, Chen H (2018) Interfacial engineering enables high efficiency with a high open-circuit voltage above 1.23 V in 2D perovskite solar cells. J Mater Chem A 6:18010–18017
35. Liu T, Jiang Y, Qin M, Liu J, Sun L, Qin F, Hu L, Xiong S, Jiang X, Jiang F, Peng P, Jin S, Lu X, Zhou Y (2019) Tailoring vertical phase distribution of quasi-two-dimensional perovskite films via surface modification of hole-transporting layer. Nat Commun 10:878
36. Zhang Y, Wang P, Tang MC, Barrit D, Ke W, Liu J, Luo T, Liu Y, Niu T, Smilgies DM, Yang Z, Liu Z, Jin S, Kanatzidis MG, Amassian A, Liu SF, Zhao K (2019) Dynamical transformation of two-dimensional perovskites with alternating cations in the interlayer space for high-performance photovoltaics. J Am Chem Soc 141:2684–2694
37. Wu GB, Zhou JY, Zhang JQ, Meng R, Wang BX, Xue BD, Leng XY, Zhang DY, Zhang XN, Bi SQ, Zhou Q, Wei ZX, Zhou HQ, Zhang Y (2019) Management of the crystallization in two-dimensional perovskite solar cells with enhanced efficiency within a wide temperature range and high stability. Nano Energy 58:706–714
38. Zhang J, Qin JJ, Wang MS, Bai YJ, Zou H, Keum JK, Tao RM, Xu HX, Yu HM, Haacke S, Hu B (2019) Uniform permutation of quasi-2D perovskites by vacuum poling for efficient, high-fill-factor solar cells. Joule 3:3061–3071
39. Wu G, Li X, Zhou J, Zhang J, Zhang X, Leng X, Wang P, Chen M, Zhang D, Zhao K, Liu SF, Zhou H, Zhang Y (2019) Fine multi-phase alignments in 2D perovskite solar cells with efficiency over 17% via slow post-annealing. Adv Mater 31:e1903889
40. Tsai H, Nie W, Blancon JC, Stoumpos CC, Asadpour R, Harutyunyan B, Neukirch AJ, Verduzco R, Crochet JJ, Tretiak S, Pedesseau L, Even J, Alam MA, Gupta G, Lou J, Ajayan PM, Bedzyk MJ, Kanatzidis MG (2016) High-efficiency two-dimensional Ruddlesden-Popper perovskite solar cells. Nature 536:312–316
41. Edri E, Kirmayer S, Mukhopadhyay S, Gartsman K, Hodes G, Cahen D (2014) Elucidating the charge carrier separation and working mechanism of CH3NH3PbI3-xClx perovskite solar cells. Nat Commun 5
42. Zhao Y, Zhu K (2014) CH3NH3Cl-assisted one-step solution growth of CH3NH3PbI3: structure, charge-carrier dynamics, and photovoltaic properties of perovskite solar cells. J Phys Chem C 118:9412–9418
43. Williams ST, Zuo F, Chueh CC, Liao CY, Liang PW, Jen AK (2014) Role of chloride in the morphological evolution of organo-lead halide perovskite thin films. ACS Nano 8:10640–10654
44. Quarti C, Mosconi E, Umari P, De Angelis F (2017) Chlorine incorporation in the CH3NH3PbI3 perovskite: small concentration, big effect. Inorg Chem 56: 74–83
45. Dar MI, Abdi-Jalebi M, Arora N, Moehl T, Gratzel M, Nazeeruddin MK (2015) Understanding the impact of bromide on the photovoltaic performance of CH3NH3PbI3 solar cells. Adv Mater 27:7221
46. Chen HR, Xia YD, Wu B, Liu F, Niu TT, Chao LF, Xing GC, Sum T, Chen YH, Huang W (2019) Critical role of chloride in organic ammonium spacer on the performance of low-dimensional Ruddlesden-Popper perovskite solar cells. Nano Energy 56:373–381
47. Feng MH, You S, Cheng NA, Du JH (2019) High quality perovskite film solar cell using methanol as additive with 19.5% power conversion efficiency. Electrochim Acta 293:356–363
48. Soe CMM, Nie WY, Stoumpos CC, Tsai H, Blancon JC, Liu FZ, Even J, Marks TJ, Mohite AD, Kanatzidis MG (2018) Understanding film formation morphology and orientation in high member 2D Ruddlesden-Popper perovskites for high-efficiency solar cells. Adv Energy Mater 8
49. Ni X, Lei L, Yu Y, Xie J, Li M, Yang S, Wang M, Liu J, Zhang H, Ye B (2019) Effect of Br content on phase stability and performance of H2N= CHNH2Pb(I1-x Br x)3 perovskite thin films. Nanotechnology 30:165402
50. Liang PW, Liao CY, Chueh CC, Zuo F, Williams ST, Xin XK, Lin J, Jen AK (2014) Additive enhanced crystallization of solution-processed perovskite for highly efficient planar-heterojunction solar cells. Adv Mater 26:3748–3754

Publisher's Note